A Minimization Approach for Constructing Generalized Barycentric Coordinates and Its Computation

Chongyang Deng* Xiali Fan † Ming-Jun Lai ‡

August 1, 2019

Abstract

We are interested in constructing more generalized barycentric coordinates(GBC) over arbitrary polygon in the 2D setting. We propose a constrained minimization over the class of infinitely differentiable functions subject to the GBC constraints of preserving linear functions and the nonnegativity condition. It includes the harmonic GBC, biharmonic GBC, maximum entropy GBC, local barycentric coordinates as special cases. We mainly show that the constrained minimization has a unique solution when the minimizing functional is strictly convex. Next we use a C^r smoothness spline function space $S_d^r(\triangle)$ with $r \geq 2$ over a triangulation $\triangle$ of a polygon of interest in $\mathbb{R}^2$ to approximate the minimizer. The minimization restricted to the spline space S_d^r certainly has a unique minimizer. Then we use the standard projected gradient descent (PGD) method to approximate the spline minimizer. To find the projection of each iteration, we shall explain an alternating projection algorithm (APA). A convergence of the APA and the convergence of the PGD with the APA will be presented. As an example of this approach, a new kind of biharmonic GBC functions which preserve the nonnegativity is defined. Finally, we have implemented the PGD method based on bivariate splines. The surfaces of many new GBC's will be shown. Some standard GBC applications will be demonstrated.

1 Introduction

Given a polygon $P_n \in \mathbb{R}^2$ of n-sides with vertices $\mathbf{v}_i, i = 1, \cdots, n$, the functions $\phi_i, i = 1, \cdots, n$ satisfying the following conditions: for any point $\mathbf{x} = (x, y) \in P_n$,

$$\begin{cases} \sum_{i=1}^n \phi_i(\mathbf{x}) & = 1 \\ \sum_{i=1}^n \phi_i(\mathbf{x})\mathbf{v}_i & = \mathbf{x} \\ \phi_i(\mathbf{x}) & \geq 0, \quad i = 1, \cdots, n \end{cases} \tag{1}$$

are called generalized barycentric coordinates (GBC). The study of generalized barycentric coordinates (GBC) started from a seminal work in [26]. Since then, there are many GBCs which have been constructed. We refer to a recent survey in [9] and a book [12] edited by leading experts K. Hormann and N. Sukumar. These GBCs have found their applications in geometric design. See, e.g. [13], [28], and etc.. In addition, they found their applications in numerical solution of partial differential equations. We refer the interested reader to [20], [23], [10], [16] and etc..

*School of Science, Hangzhou Dianzhi University, Xiasha, Hangzhou 310018, China

†13866153483@163.com. Department of Mathematics, Hangzhou Dianzhi University, Xiasha, Hangzhou 310018, China.

‡mjlai@uga.edu. Department of Mathematics, University of Georgia, Athens, GA 30602. This research is partially supported by the National Science Foundation under the grant #DMS 1521537.

In this paper, we are interested in constructing more GBC functions. Mainly, we propose to use a minimization approach to construct GBC functions. Let $p_n = \langle \mathbf{v}_1, \cdots, \mathbf{v}_n \rangle$ be an n-sided polygon with vertices $\mathbf{v}_i, i = 1, \cdots, n \in \mathbb{R}^2$. Let $f(x_1, \cdots, x_n)$ be a continuous and convex function in $\mathbb{R}^n$. Consider the following minimization problem:

$$\min\{f(\phi_1, \cdots, \phi_n) : \text{subject to } \sum_{i=1}^{n} \phi_i(\mathbf{x}) = 1, \sum_{i=1}^{n} \phi_i(\mathbf{x})\mathbf{v}_i = \mathbf{x}, \mathbf{x} \in p_n, \phi_i \geq 0, i = 1, \cdots, n\}. \quad (2)$$

For example, one can choose $f(\phi_1, \cdots, \phi_n) = \sum_{i=1}^{n} \int_{p_n} |\nabla \phi_i(\mathbf{x})|^2 d\mathbf{x}$ which leads to a harmonic GBC as explained in [14]. For another example, one can choose $f(\phi_1, \cdots, \phi_n) = \sum_{i=1}^{n} \phi_i \log(\phi_i)$ which is the minimization function for the maximum entropy GBC. See [24] and [15]. Similarly, minimizing functionals $f(\phi_1, \cdots, \phi_n) = \sum_{i=1}^{n} \int_{p_n} |\Delta \phi_i(\mathbf{x})|^2 d\mathbf{x}$ and $f(\phi_1, \cdots, \phi_n) = \sum_{i=1}^{n} \int_{p_n} |\nabla \phi_i(\mathbf{x})| d\mathbf{x}$ were used in [13] and [28], respectively. Let $\mathcal{F} = \{(\phi_1, \cdots, \phi_n) : \sum_{i=1}^{n} \phi_i(\mathbf{x}) = 1, \sum_{i=1}^{n} \phi_i(\mathbf{x})\mathbf{v}_i = \mathbf{x}, \mathbf{x} \in p_n, \phi_i \geq 0, i = 1, \cdots, n\} \subset [C^\infty(p_n)]^n$ be the feasible set. For any convex polygon p_n, it is known that Wachspress coordinates $\phi_1, \cdots, \phi_n$ in [26] satisfy the GBC conditions in (1) and the $(\phi_1, \cdots, \phi_n)$ is in $\mathcal{F}$. Therefore, the feasible set $\mathcal{F}$ is always nonempty for convex polygon p_n. For p_n is an arbitrary polygon, we know that the mean value coordinates $(\phi_1, \cdots, \phi_n)$ together with barycentric coordinates of a triangle (cf. [9]) satisfy (1) and hence, $\mathcal{F}$ is not an empty set neither. As the feasible set is not empty, the minimization (2) will have a solution. Thus we first have the following

Theorem 1 *Suppose that the minimizing function $f(\phi_1, \cdots, \phi_n)$ is a continuous and strictly convex function. Then there exists a unique minimizer $(\phi_1, \cdots, \phi_n)$ solving (2).*

See a detailed proof in the next section. This result leads to a method for constructing a set of GBC functions as long as the minimizing functional $f(\phi_1, \cdots, \phi_n)$ is a strictly convex functional. As there are many continuous and strictly convex functions available, we will have many kinds of GBC functions. For example, $f(\phi_1, \cdots, \phi_n) = \sum_{i=1}^{n} \phi_i^\alpha$ for $\alpha \geq 1$. For another example, $f(\phi_1, \cdots, \phi_n) = \sum_{i=1}^{n} \phi_i \log(\phi_i + \epsilon)$ for $\epsilon \geq 0$. When $\epsilon = 0$, it is called the maximum entropy GBC (cf. [24]). The following are more strictly convex functions: $f(\phi_1, \cdots, \phi_n) = \sum_{i=1}^{n} -\sqrt{\phi_i + \epsilon}$ for any $\epsilon \geq 0$; $f(\phi_1, \cdots, \phi_n) = \sum_{i=1}^{n} \exp(-\phi_i)$, $f(\phi_1, \cdots, \phi_n) = \sum_{i=1}^{n} -\log(\phi_i + 1)$, and etc.. Let us recall that there are other minimization approaches. For the harmonic GBC and biharmonic GBCs, the computation can be converted to the computation of Laplace equations and biharmonic equations with specified boundary conditions. See [14], [13] and [27] for detail. Indeed, the harmonic GBC ϕ_i satisfies the following Laplace equation:

$$\begin{cases} \Delta u &= 0, \quad \mathbf{x} \in p_n \\ u &= g_i, \quad \mathbf{x} \in \partial p_n, \end{cases} \quad (3)$$

where p_n is the polygon spanned by its vertices $\mathbf{v}_1, \cdots, \mathbf{v}_n$ and $g_i(\mathbf{x}) = 1$ if $\mathbf{x} = \mathbf{v}_i$ and 0 if $\mathbf{x} = \mathbf{v}_j, j \neq i$ and $g(\mathbf{x})$ is linear on the boundary of p_n. It is known the Laplace equation is the Euler-Lagrange equation of the following minimization

$$\begin{cases} \min_{u \in C^\infty(p_n)} & \int_{p_n} |\nabla u|^2, \\ u & = g_i, \quad \mathbf{x} \in \partial p_n. \end{cases} \quad (4)$$

Thus letting $f(\phi_1, \cdots, \phi_n) = \sum_{i=1}^{n} \int_{p_n} |\nabla \phi_i|^2$, we can solve (2) to find these harmonic coordinates $\phi_1, \cdots, \phi_n$. Detail can be found later.

Next we discuss how to compute these GBC functions. In general, solving the minimization (2) explicitly and analytically is very hard. Nowadays computer is so powerful. Let us propose to solve the minimization (2) numerically. One of the main purposes of this paper is to study how to solve the constrained minimization in (2). As each ϕ_i is an infinitely continuously differentiable function, we can approximate ϕ_i by using a smooth spline function. Indeed, let $\triangle$ be a triangulation of p_n and consider

$$S_d^r(\triangle) = \{s \in C^r(\triangle) : s|_T \in \mathbb{P}_d, T \in \triangle\} \tag{5}$$

be the spline space of spline functions of smooth $r \geq 1$ and degree d over triangulation $\triangle$, where $d > r$. See [18] for triangulation of any polygonal domain and spline spaces over $\triangle$. Moreover, we shall use quasi-uniform triangulations to approximate GBC functions. That is, we assume that there exists a positive number $\gamma > 0$ such that

$$\sup_{T \in \triangle} \frac{|T|}{\rho_T} \leq \gamma < \infty, \tag{6}$$

where $|T|$ is the diameter of the smallest circle containing T and ρ_T is the radius of the largest circle contained in T. Each triangulation $\triangle$ satisfies (6) is called γ-quasi-uniform triangulation. In particular, when $d \geq 3r + 2$, the spline space $S_d^r(\triangle)$ has the following nice approximation property (cf. [17] or [18]):

Theorem 2 *Suppose that $\triangle$ is a γ-quasi-uniform triangulation of polygonal domain Ω. Let $|\triangle| = \max_{T \in \triangle} |T|$ be the size of triangulation $\triangle$. Let $d \geq 3r + 2$ be the degree of spline space $S_d^r(\triangle)$. For every $u \in C^{m+1}(\overline{\Omega})$, there exists a quasi-interpolatory spline function $Q_d(u) \in S_d^r(\triangle)$ such that*

$$\|D_x^\alpha D_y^\beta (u - Q_d(u))\|_{\infty,\Omega} \leq K|\triangle|^{(m+1-s)}|u|_{m+1,\infty,\Omega} \tag{7}$$

for $\alpha + \beta = s, 0 \leq s \leq m+1$, where $0 \leq m \leq d$, K is a positive constant dependent only on γ, Ω, and d.

For convenience, fix $r \geq 1$ and $d \geq 3r + 2$. Let N be the dimension of spline space $S_d^r(\triangle) = \text{span}\{b_i, i = 1, \cdots, N\}$, where $b_i, i = 1, \cdots, N$ are linearly independent basis functions. For each generalized barycentric coordinate function ϕ_i, we write

$$\phi_i \approx s_i = \sum_{j=1}^{N} c_{ij} b_j, \quad i = 1, \cdots, n. \tag{8}$$

By Theorem 2 with $\Omega = p_n$, we know we can well approximate ϕ_i using an appropriate spline, i.e., coefficients $c_{ij}, j = 1, \cdots, N$ as soon as $|\triangle|$ sufficiently small.

Suppose that the minimizer set $(\phi_1, \cdots, \phi_n)$ has a uniform bounded $d+1$ derivative, i.e.

$$|\phi_i|_{d+1,\infty,\Omega} \leq K_1 < \infty, \quad i = 1, \cdots, n$$

for d sufficiently large, say $d \geq 5$. Let us assume that $|\triangle|$ is indeed small enough. By Theorem 2, we recast (2) as follows.

$$\min_{\substack{s_i \in S_d^r(\triangle) \\ i=1,\cdots,n}} \{f(\phi_1, \cdots, \phi_n) : \text{subject to } \sum_{i=1}^{n} s_i(\mathbf{x}) = 1, \sum_{i=1}^{n} s_i(\mathbf{x})\mathbf{v}_i = \mathbf{x}, \mathbf{x} \in p_n, s_i \geq 0, i = 1, \cdots, n\}. \tag{9}$$

In the remaining of this paper, we shall address the solution to the minimization (9) above. The existence and uniqueness of the minimizer of (9) follows from the same arguments of the proof of Theorem 1. In the following, we mainly discuss the computation of the minimizer. Note that one of the GBC conditions in (1) can be rewritten as follows:

$$1 = \sum_{i=1}^{n} s_i(\mathbf{x}) = \sum_{j=1}^{N} (\sum_{i=1}^{n} c_{ij}) b_j \tag{10}$$

Since we can choose $\sum_{j=1}^{N} b_j = 1$, due to the linear independence of $b_j, j = 1, \cdots, N$, we have

$$\sum_{i=1}^{n} c_{ij} = 1, \quad \forall j = 1, \cdots, N. \tag{11}$$

One can write $x = \sum_{j=1}^{N} c_{x,j} b_j(\mathbf{x})$ and $y = \sum_{j=1}^{N} c_{y,j} b_j(\mathbf{x})$. Then the other condition in (1) can be written as

$$\sum_{i=1}^{n} \mathbf{v}_i \sum_{j=1}^{N} c_{ij} b_j(\mathbf{x}) = \sum_{j=1}^{N} b_j(\mathbf{x}) \sum_{i=1}^{n} \mathbf{v}_i c_{ij} = \sum_{j=1}^{N} b_j(\mathbf{x})(c_{x,j}, c_{y,j}). \tag{12}$$

It follows that

$$\sum_{i=1}^{n} \mathbf{v}_i c_{ij} = (c_{x,j}, c_{y,j}), \quad j = 1, \cdots, N. \tag{13}$$

Finally, the nonnegativity condition and boundedness condition $0 \leq \phi_i \leq 1$ can be imposed by

$$c_{ij} \in [0, 1], j = 1, \cdots, N, i = 1, \cdots, n. \tag{14}$$

Then the minimization problem (2) can be recast as follows. Write

$$F(c_{1,1}, \cdots, c_{1,N}, \cdots, c_{n,1}, \cdots, c_{n,N}) = f(\sum_{j=1}^{N} c_{1,j} b_j, \cdots, \sum_{j=1}^{N} c_{n,j} b_j)$$

to be the new format for the minimization function in (2) and $\mathbf{c} = (c_{1,1}, \cdots, c_{1,N}, \cdots, c_{n,1}, \cdots, c_{n,N})$ be the solution vector, our new minimization problem is

$$\begin{aligned} \min_{\mathbf{c} \in \mathbb{R}^{nN}} \{ F(\mathbf{c}) : & \sum_{i=1}^{n} c_{ij} = 1, \sum_{i=1}^{n} \mathbf{v}_i c_{ij} = (c_{x,j}, c_{y,j}), j = 1, \cdots, N, \\ & 0 \leq c_{ij} \leq 1, j = 1, \cdots, N, i = 1, \cdots, n \}. \end{aligned} \tag{15}$$

To this end we shall discuss a numerical method to solve (15) to approximate the minimizers $\phi_1, \cdots, \phi_n$ in (2). In particular, for harmonic and biharmonic GBCs, we will present a simpler minimization than the one in (15) to compute them.

Finally, our contributions in this paper can be summarized as follows. (1) We develop a minimization approach to construct more new GBC functions. This approach extends the construction of harmonic GBCs, biharmonic GBCs, minimal entropy GBCs, local Barycentric Coordinates to a more general setting. (2) since the GBCs are belong to C^{∞} differentiable functions, we employ finite dimensional spaces of smooth spline functions to approximate them. That is, we explain how to use bivariate spline functions to approximate these minimizers. Trivariate spline approximation to these GBC functions will be discussed in a further coming paper as the computation is much more

complicated. This approach enable us to have a smoother approximation of GBC functions than the finite element method. One can see clearly from the surface deformation (in the last section) that the contour lines are smooth during the deformation steps. (3) Due to the minimization is a constrained minimization, an alternating projection method will be used to project gradients. A convergence analysis of the alternating projections between a convex set and linear affine spaces will be provided. Although the convergence of alternating projection algorithm between linear affine spaces and between convex sets via Dykstra technique is well-known, the convergence of APA between linear affine spaces and convex sets is new to the best of the authors' knowledge. (4) In particular, the minimization (2) with an appropriate functional leads to another kind of biharmonic GBC functions which guarantees to have nonnegative property. That is, we explain how to use the alternating projection approach to find nonnegative biharmonic GBCs. This improves the biharmonic GBCs presented in [13] and [27], where the nonnegativity is not always possible. Based on this minimization approach, examples of several new and existing GBC functions will be presented together with their numerical applications.

2 Main Existence Results

In this section we shall first give a proof to our main existence result.

Theorem 3 *Suppose that the minimizing function $f(\phi_1, \cdots, \phi_n)$ is a continuous and strictly convex function. Then there exists a unique minimizer $(\phi_1, \cdots, \phi_n)$ solving (2).*

Proof. Let $\Omega = \{(\phi_1, \cdots, \phi_n) : 0 \leq \phi_i \leq 1, \forall i = 1, \cdots, n\}$ be a bounded domain in $\mathbb{R}^n$. Our minimizing function f is defined over Ω. Since f is a continuous function, we know that f is bounded over Ω and achieves the minimum in Ω.

As explained in the Introduction section, the feasible set $\mathcal{F}$ is nonempty. Next we will prove that any local minimum is the global minimum. Assuming that $\Phi' \in \Omega$ is a local minimum, but is not the global minimum on Ω. That is, $f(\Phi') > f(\Phi^*)$, where Φ^* is the global minimum point. Then there is θ such that $(1-\theta)\Phi' + \theta\Phi^* \in \Omega$. Because f is a convex function, we can obtain

$$f((1-\theta)\Phi' + \theta\Phi^*) \leq (1-\theta)f(\Phi') + \theta f(\Phi^*) < (1-\theta)f(\Phi') + \theta f(\Phi') = f(\Phi')$$

which contradicts to the fact that Φ' is a local minimizing point as $\theta \in (0,1)$ can be arbitrarily small and $(1-\theta)\Phi' + \theta\Phi^*$ can be within any neighborhood of Φ'. Therefore the local minimum is just the global minimum. □

Similarly, for the finite dimensional minimization (9), i.e. (15) we have

Theorem 4 *Suppose that the minimizing function $F(\mathbf{c}), \mathbf{c} \in \mathbb{R}^{nN}$ in (15) is a continuous and strictly convex function. If the size $|\triangle|$ of the underlying triangulation $\triangle$ is small enough, then there exists a unique vector $\mathbf{c}^*$ solving (15). That is, there exists a unique minimizer $(s_1, \cdots, s_n) \in [S_d^r(\triangle)]^n$ solving (9).*

Proof. We simply solve Laplace equation in (3) based on a spline space $S_d^r(\triangle)$ with $r \geq 1$ and $d \geq 3r+2$ for each $i = 1, \cdots, n$. Therefore, the feasible set is not empty. The rest of the proof is the same as above Theorem 3. □

Next we comment on computing GBC by solving (2).

Remark 1 *When constructing GBCs, one often combines two constraints in (1) into one. That is, one uses*

$$\sum_{i=1}^{n} \phi_i(\mathbf{v}_i - \mathbf{x}) = 0. \tag{16}$$

We have to point out that this is not always possible. Consider a minimizing functional $f(\phi_1, \cdots, \phi_n) = \sum_{i=1}^{n} \phi_i^2$. *Then the following minimization problem*

$$\min\{\sum_{i=1}^{n} \phi_i^2 : (16) \text{ and } \phi_i \geq 0\} \tag{17}$$

has a unique solution $\phi_1 = \phi_2 = \cdots = \phi_n = 0$. *However, the minimization (2) has a set of solution which are not zero. See an example in the Numerical Experimental Section. This explains that the minimization with only (16) does not always work.*

Remark 2 *Another confused point in solving (2) is to use Lagrange multiplier method without using the constraints* $\phi_i \geq 0, i = 1, \cdots, n$. *The solution could be negative as seen the following explanation. We again use* $f(\phi_1, \cdots, \phi_n) = \sum_{i=1}^{n} \phi_i^2$ *as an example. Using Lagrange multiplier method, we let*

$$F(\phi_1, \cdots, \phi_n) = \sum_{i=1}^{n} \phi_i^2 + \nu_1(\sum_{i=1}^{n} \phi_i - 1) + \nu_2(\sum_{i=1}^{n} \phi_i v_{i,x} - x) + \nu_3(\sum_{i=1}^{n} \phi_i v_{i,y} - y).$$

We have the following n+3 equations:

$$\begin{aligned} 2\phi_i + 2\nu_1 + \nu_2 v_{i,x} + \nu_3 v_{i,y} = 0, i = 1, \cdots, n \\ \sum_{i=1}^{n} \phi_i = 1, \sum_{i=1}^{n} \phi_i v_{i,x} = x, \sum_{i=1}^{n} \phi_i v_{i,y} = y. \end{aligned} \tag{18}$$

In matrix form, we have

$$\begin{bmatrix} 2 & 0 & \cdots & 0 & 1 & v_{1,x} & v_{1,y} \\ 0 & 2 & \ddots & \vdots & 1 & v_{2,x} & v_{2,y} \\ \vdots & \ddots & \ddots & 0 & \vdots & \vdots & \vdots \\ 0 & \cdots & \cdots & 2 & 1 & v_{n,x} & v_{n,y} \\ 1 & 1 & \cdots & 1 & 0 & 0 & 0 \\ v_{1,x} & v_{2,x} & \cdots & v_{n,x} & 0 & 0 & 0 \\ v_{2,y} & v_{2,y} & \cdots & v_{n,y} & 0 & 0 & 0 \end{bmatrix} \begin{bmatrix} \phi_1 \\ \phi_2 \\ \vdots \\ \phi_n \\ \nu_1 \\ \nu_2 \\ \nu_3 \end{bmatrix} = \begin{bmatrix} 0 \\ 0 \\ \vdots \\ 0 \\ 1 \\ x \\ y \end{bmatrix}.$$

Letting I *be the identity matrix of size* $n \times n$, $\mathbf{0}$ *be the zero matrix of size* 3×3, *and*

$$A = \begin{bmatrix} 1 & 1 & \cdots & 1 \\ v_{1,x} & v_{2,x} & \cdots & v_{n,x} \\ v_{2,y} & v_{2,y} & \cdots & v_{n,y} \end{bmatrix}, \Phi = [\phi_1, \cdots, \phi_n]^\top,$$

and $\nu = [\nu_1, \nu_2, \nu_3]^\top$ *and* $X = [1, x, y]^\top$, *the matrix can be recast as*

$$\begin{bmatrix} 2I & A^\top \\ A & \mathbf{0} \end{bmatrix} = \begin{bmatrix} \Phi \\ \nu \end{bmatrix} = \begin{bmatrix} \mathbf{0} \\ X \end{bmatrix}.$$

The solution is

$$\begin{bmatrix} \Phi \\ \nu \end{bmatrix} = \begin{bmatrix} \frac{1}{2}I & A^\top(AA^\top)^{-1} \\ 0 & -2(AA^\top)^{-1} \end{bmatrix} \begin{bmatrix} \mathbf{0} \\ X \end{bmatrix}.$$

That is, $\Phi = A^\top(AA^\top)^{-1}X$ *and each entry of* Φ *is a linear polynomial. Our computation shows that some entries can be negative over a convex polygon* p_n.

3 A Bivariate Spline Method for Solution to (15)

In this section, we describe a computational method for (15). Following the computational method of multivariate splines discussed in [3], we mainly use the spline basis for $S_d^{-1}(\triangle)$ and then couple with smoothness constraints for the coefficients of a spline function in $S_d^{-1}(\triangle)$ to form a spline function in $S_d^r(\triangle)$ for a fixed smoothness $r \geq 0$. That is, for each triangle $T \in \triangle$, let $\lambda_1, \lambda_2, \lambda_3$ be the barycentric coordinates with respect to T. Define degree d Bernstein-Bézier polynomials by

$$B_{ijk}^T = \frac{d!}{i!j!k!}\lambda_1^i\lambda_2^j\lambda_3^k \geq 0, \quad i+j+k=d. \tag{19}$$

Then $B_{ijk}^T, i+j+k=d, T \in \triangle$ form a basis for $S_d^{-1}(\triangle)$. We let $\mathbf{s} = (c_{ijk}^T, i+j+k=d, T \in \triangle)$ be the coefficient vector for a spline function $s \in S_d^{-1}(\triangle)$:

$$s = \sum_{T\in\triangle}\sum_{i+j+k=d} c_{ijk}^T B_{ijk}^T. \tag{20}$$

Note that $\sum_{i+j+k=d} B_{ijk}^T = 1$. Together with condition in (19), $0 \leq c_{ijk}^T \leq 1$ will imply that $0 \leq s \leq 1$ over p_n.

When $s \in S_d^r(\triangle)$ for a smoothness order $r \geq 0$, its coefficient vector $\mathbf{s}$ satisfies smoothness conditions across each interior edge of $\triangle$. These smoothness conditions are linear and we can write them in terms of system of linear equations: $H\mathbf{s} = 0$, where H is called a smoothness matrix. See [3] and [18] for detail.

In this setting, we have to rewrite our minimization (15). To be more precisely, let $N = \frac{1}{2}(d+1)(d+2)\#(\triangle)$, where $\#(\triangle)$ stands for the number of triangles in $\triangle$. As we have to approximate n functions ϕ_i, we use s_i to approximate ϕ_i and let us consider all coefficient vectors $\mathbf{s}_i, i = 1, \cdots, n$ together as a new vector: $\mathbf{c} = (\mathbf{s}_1; \mathbf{s}_2; \cdots; \mathbf{s}_n) \in \mathbb{R}^{nN}$. Since $s_i \in S_d^r(\triangle)$, we let $\mathbf{H} = (H; H; \cdots; H)$ such that $\mathbf{Hc} = 0$ stands for the smoothness constraints for all $s_1, \cdots, s_n$.

Next note that $B_{ijk}^T, i+j+k=d, T \in \triangle$ satisfy the property of the partition of unit. That is,

$$1 = \sum_{T\in\triangle}\sum_{i+j+k=d} B_{ijk}^T, \tag{21}$$

where B_{ijk}^T is only defined on the interior T and is zero outside of T. Then the conditions in (11) imply that $\sum_{i=1}^n s_{ij} = 1$, $j = 1, \cdots, N$ if $\mathbf{s}_i = (s_{i1}, \cdots, s_{iN})^\top$. Also, it is known that x, y can be reproduced by spline functions in $S_d^r(\triangle)$ with $d \geq 1$. In fact, let $\mathbf{u}_\ell = (x_\ell, y_\ell), \ell = 1, 2, 3$ be the vertices of a triangle T. Then

$$x = \sum_{i+j+k=d} \frac{1}{d}(ix_1 + jx_2 + kx_3)B_{ijk}^T \text{ and } y = \sum_{i+j+k=d} \frac{1}{d}(iy_1 + jy_2 + ky_3)B_{ijk}^T \tag{22}$$

For convenience, let us write $c_{x,i}, i = 1, \cdots, N$ be the values $\frac{1}{d}(ix_1 + jx_2 + kx_3), i+j+k=d, T \in \triangle$. Similar for $c_{y,i}, i = 1, \cdots, N$.

Therefore, the feasible set of (15) can be written precisely as follows: recalling $\mathbf{v}_i = (x_i, y_i), i =$

$1, \cdots, n$ are vertices of polygon p_n,

$$\begin{aligned}\mathcal{F}_+ = \{\mathbf{c} \in \mathbb{R}^{nN} :& \mathbf{c} \geq 0, \mathbf{H}\mathbf{c} = 0, \\ & \sum_{i=1}^{n} s_{ij} = 1, s_{ij} \geq 0, \forall j = 1, \cdots, N \\ & \sum_{i=1}^{n} s_{ij} x_i = c_{x,j}, \sum_{i=1}^{n} s_{ij} y_i = c_{y,j}, \forall j = 1, \cdots, N\}\end{aligned} \tag{23}$$

be a new feasible set.

Suppose that the minimizing functional F defined in (15) is differentiable. It is standard to use the projected gradient method which can be described in Algorithm 1.

Algorithm 1 (Projected Gradient Method) *Given a convex feasible set $\mathcal{F}_+$ and a convex objective function $F(\cdot)$, we solve the minimization in (15) by using the following iterative step: starting with an initial guess $\mathbf{x}^{(1)}$, find*

$$\mathbf{x}^{(k+1)} = \mathbb{P}_{\mathcal{F}_+}(\mathbf{x}^{(k)} - h_k \nabla F(\mathbf{x}^{(k)})), \tag{24}$$

where the operator $\mathbb{P}_{\mathcal{F}_+}$ is the projection operator which maps a vector $\mathbf{x} \in \mathbb{R}^{nM}$ to the convex set $\mathcal{F}_+$ and $h_k > 0$ is a step size.

To use Algorithm 1, let us first discuss how to find the projection $\mathbb{P}_{\mathcal{F}_+}$. We will use the alternating projection algorithm (APA) to approximate the projection $\mathbb{P}_{\mathcal{F}_+}(\mathbf{y})$ for any nonzero vector $\mathbf{y} \in \mathbb{R}^{nN}$. To this end, let us review some basic properties of hyperplanes and their projections. All details can be found in [6]. Let $X = \mathbb{R}^{nN}$ for simplicity.

Definition 1 (Hyperplanes) *A hyperplane in a Hilbert space X is any set of the form*

$$H = \{\mathbf{x} \in X : \quad \langle \mathbf{x}, \mathbf{h} \rangle = c\} \tag{25}$$

for a vector $\mathbf{h} \neq 0$ and a value $c \in \mathbb{R}$.

Note that a hyperplane H is never empty. Indeed, since $\mathbf{h} \neq 0$, there exists a vector $\mathbf{y}$ such that $\langle \mathbf{y}, \mathbf{h} \rangle = d \neq 0$. It follows that $\mathbf{x} = c\mathbf{y}/d \in H$.

Distance to Hyperplane Let H be a hyperplane given in (25). Then the distance of any point $\mathbf{p} \in X$ to the hyperplane H is

$$\text{dist}(\mathbf{p}, H) = \frac{1}{\|\mathbf{h}\|} |\langle \mathbf{p}, \mathbf{h} \rangle - c|. \tag{26}$$

Let us find the projection operator $\mathcal{P}_H$. For any $\mathbf{y} \in X$, let

$$\mathcal{P}_H(\mathbf{y}) = \mathbf{y} - \mathbf{h} \frac{\langle \mathbf{y}, \mathbf{h} \rangle - c}{\|\mathbf{h}\|^2} \tag{27}$$

which is the projection of $\mathbf{y}$ onto H. Indeed, we can easily check that $\|\mathbf{y} - \mathcal{P}_H(\mathbf{y})\| = \text{dist}(\mathbf{y}, H)$. In general, we have multiple hyperplanes and we need to find the projection operator to the intersection of multiple hyperplanes. That is, let

$$\mathcal{H}_m = \{\mathbf{x} \in X : A\mathbf{x} = \mathbf{b}\}$$

be the intersection of multiple hyperplanes, where A is an observation matrix of size $m \times nN$ and $\mathbf{b} \in \mathbb{R}^m$. When $m < nN$, the intersection $\mathcal{H}_m$ is nonempty. For any point $\mathbf{p} \in X$, finding its projection to $\mathcal{H}_m$ is a least squares problem: $\min\{\|\mathbf{p} - \mathbf{x}\| : \mathbf{x} \in \mathcal{H}_m\}$.

Theorem 5 *For any $\mathbf{p} \in X$, the projection $\mathbb{P}_{\mathcal{H}_m}(\mathbf{p})$ is given by*

$$\mathbb{P}_{\mathcal{H}_m}(\mathbf{p}) = \mathbf{p} - A^\top (AA^\top)^{-1}(A\mathbf{p} - \mathbf{b}) \tag{28}$$

if A is of full rank. If A is not of full rank, we write $A = U\Sigma V^\top$ and we have

$$\mathbb{P}_{\mathcal{H}_m}(\mathbf{p}) = \mathbf{p} - A^\top U(\Sigma_+^{-2})U^\top(A\mathbf{p} - \mathbf{b}). \tag{29}$$

Proof. It is easy to see $\mathbb{P}_{\mathcal{H}_m}(\mathbf{p}) \in \mathcal{H}_m$. Next let $\mathrm{Null}(A) = \{\mathbf{x} \in X : A\mathbf{x} = 0\}$ be the null space of A. For any nonzero $\mathbf{x} \in \mathrm{Null}(A)$ and $\alpha \in \mathbb{R}$, we know $\mathbf{p}^* + \alpha\mathbf{x} \in \mathcal{H}_m$. Now we claim that

$$\|\mathbf{p} - \mathbf{p}^*\| = \min_\alpha \|\mathbf{p} - (\mathbf{p}^* + \alpha\mathbf{x})\|,$$

where $\mathbf{p}^*$ is the vector on the right-hand side of the equation in (28). Indeed, we can easily verify that

$$\langle \mathbf{p} - \mathbf{p}^*, \mathbf{x} \rangle = 0$$

since $\mathbf{x} \in \mathrm{Null}(A)$. Therefore, we have the claim. □

Returning to our computational problem, let us consider the constraints: (11) and (13). Define

$$H_0 = \{\mathbf{c} \in X : \mathbf{H}\mathbf{c} = 0\}$$

and

$$H_1 = \{\mathbf{c} \in X : \sum_{i=1}^{n} s_{ij} = 1, \forall j = 1, \cdots, N\}$$

which is the intersection of hyperplanes. Similarly, we define

$$H_x = \{\mathbf{c} \in X : \sum_{i=1}^{n} s_{ij}x_i = c_{x,j}, \forall j = 1, \cdots, N\}$$

and

$$H_y = \{\mathbf{c} \in X : \sum_{i=1}^{n} s_{ij}y_i = c_{y,j}, \forall j = 1, \cdots, N\}$$

where $\mathbf{v}_i = (x_i, y_i), i = 1, \cdots, n$ are vertices of the polygon p_n. Finally, the nonnegative condition, i.e. $\mathbf{c} \geq 0$ can be found easily. Let

$$H_+ = \{\mathbf{c} \in X : \mathbf{c} \geq 0\}.$$

Define $\mathbb{P}_0, \mathbb{P}_1, \mathbb{P}_x, \mathbb{P}_y, \mathbb{P}_+$ to be the projections to linear spaces H_0, H_1, H_x, H_y, H_+, respectively. We now introduce the alternating projection method which is also called von Neumann algorithm invented in 1933 (cf. [6]).

In fact, the above algorithm can be simplified. We use Theorem 5 to define the projection $\mathbb{P}_{0,1,x,y}$ mapping any point $\mathbf{p} \in X$ into the subspace

$$H_{0,1,x,y} = H_0 \cap H_1 \cap H_x \cap H_y.$$

We now show the following

Algorithm 2 (Alternating Projection Method) *Let* $\mathbf{p}^{(1)} = \mathbf{p} \in \mathbb{R}^{nM}$ *be a vector. For* $k = 1, \cdots,$, *we do the following*

$$\begin{aligned} \mathbf{u} &= \mathbb{P}_0(\mathbf{p}^{(k)}) \\ \mathbf{v} &= \mathbb{P}_1(\mathbf{u}) \\ \mathbf{w} &= \mathbb{P}_x(\mathbf{v}) \\ \mathbf{x} &= \mathbb{P}_y(\mathbf{w}) \\ \mathbf{p}^{(k+1)} &= \mathbb{P}_+(\mathbf{x}) \end{aligned} \tag{30}$$

until $k >$ *a fixed number of iteration.*

Theorem 6 *Fix* $r \geq 1$. *Suppose* $d \geq 1$ *is sufficiently large. Then the intersection* $H_{0,1,x,y}$ *is not empty.*

Proof. Consider the number of equations for H_0 first. For simplicity, let us say $r = 1$. Then there are $2d + 1$ smoothness conditions across each interior edge of triangulation. By Euler's relation, letting E_I be the number of interior edges and $\#(\triangle)$ be the number of triangles in $\triangle$. Then we know $E_I/3 = V_I + V_b/3 - 1$ and $\#(\triangle)/2 = V_I + V_b/2 - 1$. That is,

$$E_I \leq 3/2\#(\triangle).$$

Thus, $\mathbf{Hc} = 0$ has $n(2d + 1)E_I$ smoothness condition equations which is less than or equal $n(2d + 1)3\#(\triangle)/2$. For H_1, H_x, H_y, these are 3N linear equations. In total, we have $n(2d+1)3\#(\triangle)/2+3N$ equations with nN variables. Recall $N = (d + 1)(d + 2)\#(\triangle)/2$. When $d \geq 4$, we have $n(2d + 1)3\#(\triangle)/2 < N$. Hence, we have $n(2d+1)3\#(\triangle)/2+3N < 4N$ equations with nN unknowns. For GBCs over polygon p_n with $n \geq 4$, the total system of linear equations, i.e. all linear constraints from H_0, H_1, H_x, H_y is underdetermined. As the underdetermined linear system many solutions, the intersection $H_0 \cap H_1 \cap H_x \cap H_y$ is not empty. We can use (28) or (29) to find the projections to H_0, H_1, H_2, H_3, the subspace of vectors satisfying (11) and (13). □

Then Algorithm 2 can be rewritten as follows.

Algorithm 3 (Alternating Projection Method(II)) *Let* $\mathbf{p}^{(1)} = \mathbf{p} \in \mathbb{R}^{nM}$ *be a vector. For* $k = 1, \cdots,$, *we do the following*

$$\begin{aligned} \mathbf{u}^{(k)} &= \mathbb{P}_{0,1,x,y}(\mathbf{p}^{(k)}) \\ \mathbf{p}^{(k+1)} &= \mathbb{P}_+(\mathbf{u}^{(k)}) \end{aligned} \tag{31}$$

until $k >$ *a fixed number of iteration.*

We now show that the above algorithm, Algorithm 3 is convergent and the rate of convergence is linear. That is, we have

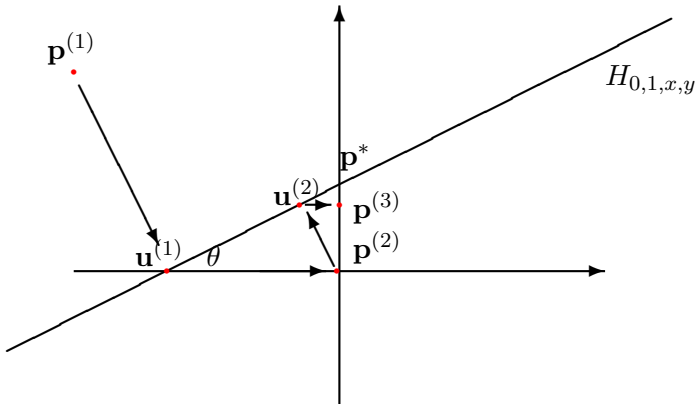

Figure 1: The convex set H_+ is the first quadrant, the hyperplane $H_{0,1,x,y}$ is the line, $\mathbf{p}^{(k)}, \mathbf{u}^{(k)}$'s are iterative points based on (31). $\mathbf{p}^*$ is the projection of $\mathbf{p}^{(1)}$ in the intersection of H_+ and $H_{0,1,x,y}$.

Theorem 7 *Let $\mathbf{p}^{(k+1)}$ be the output of the iteration from Algorithm 3. Let $\mathbf{p}^* = \mathbb{P}_{\mathcal{F}_+}(\mathbf{p})$. Then there exists a positive constant $\alpha < 1$ and a positive constant $C > 0$*

$$\|\mathbf{p}^{(k+1)} - \mathbf{p}^*\| \to C\alpha^k, \ \text{as } k \to \infty, \tag{32}$$

where α is dependent on the angles among the subspaces H_0, H_1, H_x, H_y, H_+.

Proof. We use the graph in Figure 1 to guide our proof. By the similar triangles, we have

$$\frac{\|\mathbf{p}^{(3)} - \mathbf{p}^*\|}{\|\mathbf{p}^{(2)} - \mathbf{p}^*\|} = \frac{\|\mathbf{u}^{(2)} - \mathbf{p}^*\|}{\|\mathbf{u}^{(1)} - \mathbf{p}^*\|} = 1 - \cos^2(\theta),$$

where we have used the fact that $\|\mathbf{u}^{(2)} - \mathbf{p}^*\| = \|\mathbf{u}^{(1)} - \mathbf{p}^*\| - \|\mathbf{u}^{(1)} - \mathbf{p}^*\|\cos^2(\theta)$ and θ is shown in Figure 1. That is, $\|\mathbf{p}^{(3)} - \mathbf{p}^*\| = (1 - \cos^2(\theta))\|\mathbf{p}^{(2)} - \mathbf{p}^*\|$. We repeat this argument to have the convergence results in (32) with $\alpha = 1 - \cos^2(\theta)$. This completes the proof □

We remark that the convergence of the alternating projection algorithm between two linear hyerplanes was established many decades ago. Also, the convergence of the alternating projection algorithm between two convex sets via Dykstra's approach was also established. See proofs of these two cases in [6]. However, the proof of the convergence of the alternating projection algorithm between one hyperplane and one convex was not found in [6]. According to [7], this result have not been established to the best of the authors and Prof. Frank Deutsch. Thus, we present a proof to this special case for our application in Theorem 7. In addition, we remark that if one switch the order of projections, i.e.

$$\begin{cases} \mathbf{u}^{(k)} & = \mathbb{P}_+(\mathbf{p}^{(k)}) \\ \mathbf{p}^{(k+1)} & = \mathbb{P}_{0,1,x,y}(\mathbf{u}^{(k)}), \end{cases} \tag{33}$$

then the resulting alternating projection algorithm may not converge. See Figure 2.

Once we have the projection $\mathbb{P}_{\mathcal{F}_+}$ for the constraints in (15). The iterative steps in the projected gradient Algorithm 1 are well defined. Let us explicit the projection in Algorithm 1 and combine the alternating projection Algorithm 3 together to have

Let us give a theorem to ensure its convergence of Algorithm 4. To this end, we need concepts on differentiable function F. F is L-Lipschitz differentiable if

$$\|\nabla F(\mathbf{y}) - \nabla F(\mathbf{x})\| \le L\|\mathbf{y} - \mathbf{x}\|, \quad \forall \mathbf{x}, \mathbf{y} \in X. \tag{34}$$

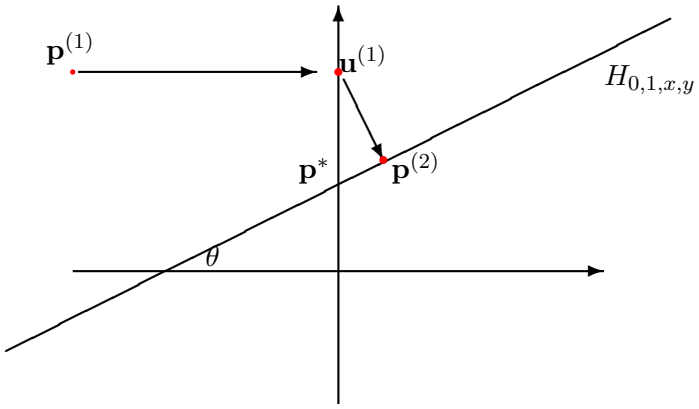

Figure 2: The convex set H_+ is the first quadrant, the hyperplane $H_{0,1,x,y}$ is the line, $\mathbf{u}^{(1)}, \mathbf{p}^{(2)}$'s are iterative points based on (33). Iterations will terminate at $\mathbf{p}^{(2)}$ which is not the projection $\mathbf{p}^*$ of $\mathbf{p}^{(1)}$

Algorithm 4 (Projected Gradient Method (II)) *Given a convex feasible set $\mathcal{F}_+$ and a convex objective function $F(\cdot)$, we solve the minimization in (15) by using the following iterative step: starting with an initial guess $\mathbf{x}^{(1)}$, find*

$$\begin{aligned} \mathbf{u}^{(k)} &= \mathbf{x}^{(k)} - h_k \nabla F(\mathbf{x}^{(k)}) \\ \mathbf{x}^{(k+1)} &= \text{ output of Algorithm 3 for a fixed number of iterations} \end{aligned}$$

unit a stopping criterion is met.

Also, F is ν-strongly convex if

$$F(\mathbf{y}) \geq F(\mathbf{x}) + \langle \nabla F(\mathbf{x}), \mathbf{y} - \mathbf{x} \rangle + \frac{\nu}{2} \|\mathbf{x} - \mathbf{y}\|^2, \forall \mathbf{x}, \mathbf{y} \in X. \tag{35}$$

We are now ready to show the convergence of Algorithm 1. The proof is a modification of the standard proof of the convergence of Algorithm 1 in optimization.

Theorem 8 *Suppose that f is L-Lipschitz differentiable and f is ν-strongly convex. Let $\mathbf{x}^*$ be the minimizer of the problem (15). Suppose that the number of inner iterations in Algorithm 3 is fixed, say $m \geq 1$. Then*

$$\|\mathbf{x}^{(k+1)} - \mathbf{x}^*\| \leq C\gamma^k, \quad \forall k \geq 1, \tag{36}$$

where C is a positive constant. Here the step size $h_k = h > 0$ is small enough.

Proof. We first claim that $\mathbf{x}^* = \mathbb{P}_{\mathcal{F}_+}(\mathbf{x}^* - h\nabla f(\mathbf{x}^*))$. Indeed, for any minimizer $\mathbf{w}^* \in W^*$, the set of all minimizers, we have

$$\langle \nabla F(\mathbf{w}^*), \mathbf{w} - \mathbf{w}^* \rangle \geq 0 \tag{37}$$

for all $\mathbf{w} \in \mathcal{F}_+$, where $W^* \subset \mathcal{F}_+$ is the set of all minimizers. Denote by $\mathbf{y} = \mathbb{P}_{\mathcal{F}_+}(\mathbf{x}^* - h\nabla f(\mathbf{x}^*))$. Then we know

$$\langle \mathbf{y} - (\mathbf{x}^* - h\nabla F\mathbf{x}^*)), \mathbf{y} - \mathbf{x} \rangle \leq 0, \quad \forall \mathbf{x} \in \mathcal{F}_+.$$

From (37), we can see that $\mathbf{y} = \mathbf{x}^*$ as $h > 0$ if we choose $\mathbf{x} = \mathbf{x}^*$.

Now we have

$$\|\mathbf{x}^{(k+1)} - \mathbf{x}^*\|^2 = \|\mathbb{P}_{\mathcal{F}_+}(\mathbf{x}^{(k)} - h_k \nabla F(\mathbf{x}^{(k)})) - \mathbb{P}_{\mathcal{F}_+}(\mathbf{x}^* - h_k \nabla F(\mathbf{x}^*))\|.$$

Since $\mathbb{P}_{\mathcal{F}_+}$ is a projection, one knows that $\mathbb{P}_{\mathcal{F}_+}$ is non-expansive, that is, $\|\mathbb{P}_{\mathcal{F}_+}(\mathbf{x}) - \mathbb{P}_{\mathcal{F}_+}(\mathbf{y})\| \leq \|\mathbf{x} - \mathbf{y}\|$. We leave the proof to the interested reader. Thus the right-hand side of the above equation yields

$$\|\mathbf{x}^{(k+1)} - \mathbf{x}^*\|^2 \leq \|\mathbf{x}^{(k)} - \mathbf{x}^* - h_k(\nabla f(\mathbf{x}^{(k)}) - \nabla f(\mathbf{x}^*))\|^2.$$

and hence, by using the strong convexity,

$$\begin{array}{ll} & \|\mathbf{x}^{(k+1)} - \mathbf{x}^*\|^2 \\ \leq & \|\mathbf{x}^{(k)} - \mathbf{x}^*\|^2 - 2h_k\langle \mathbf{x}^{(k)} - \mathbf{x}^*, \nabla f(\mathbf{x}^{(k)}) - \nabla f(\mathbf{x}^*)\rangle + h_k^2 \|\nabla f(\mathbf{x}^{(k)}) - \nabla f(\mathbf{x}^*)\|^2 \\ \leq & \|\mathbf{x}^{(k)} - \mathbf{x}^*\|^2 (1 - 2h_k\nu + h_k^2 L^2). \end{array}$$

It follows that for all $k \geq 1$, letting $\gamma = (1 - 2h\nu + h^2L^2)^{1/2} < 1$, we have

$$\|\mathbf{x}^{(k+1)} - \mathbf{x}^*\| \leq \gamma \|\mathbf{x}^{(k)} - \mathbf{x}^*\| \leq \cdots \leq \gamma^k \|\mathbf{x}^{(1)} - \mathbf{x}^*\|.$$

for all $k \geq 1$, where $h_k = h < 1$. □

We have a few remarks in order.

Remark 3 *We can use Algorithm 4 even when F is not strongly convex. As long as F is convex and is Lipschitz differentiable, Algorithm 4 will converge. The rate of convergence of Algorithm 4 when F is Lipschitz differentiable is $o(1/k)$, where k is the number of iterative steps. Here we say the kth error $e_k = o(1/k)$ if $ke_k \to 0$. See [5]. Furthermore, we can accelerate the iterations by using the well-known Nesterov's acceleration technique (cf. [21] and [22]) or the recent improved Attouch-Peypouquet acceleration technique(cf. [2]). Then the rate of convergence will be $o(1/k^2)$ which is slightly better than the rate of convergence based on Nesterov's acceleration technique.*

Remark 4 *Note that when p_n is not convex, the feasible set $\mathcal{F}_+$ is not convex and hence, the convergence of Algorithm 1 is not guaranteed. That is, the minimizer may not satisfy (1) at the reentry vertex of p_n in general. How to tackle this situation will be addressed in the next section.*

Remark 5 *A disadvantage of this approach is that the system of linear equations for linear preservation constraints for all GBC functions can be very large when the number n of sides of a polygon p_n is large. Harmonic and biharmonic GBCs have an advantage that each GBC function can be numerically solved individually and hence, can be done in parallel. Thus it is worthy further developing a more efficient numerical method for our minimization approach.*

4 Numerical New and Known GBC Functions

In this section, we use bivariate splines to solve the minimization (15) to produce some new and known GBC functions. The implementation of bivariate splines can be found in [3]. In the following examples, we shall use $d = 8$ and $r = 2$ as well as $d = 5$ and $r = 1$ with appropriate triangulation of polygonal domain p_n for $n \geq 4$. We shall begin with biharmonic functionals and then study the following two minimizing functionals

$$f(\phi_1, \cdots, \phi_n) = \frac{1}{2} \sum_{i=1}^{n} \int_{p_n} |\phi_i(\mathbf{x})|^2 d\mathbf{x},$$

$$f(\phi_1, \cdots, \phi_n) = \sum_{i=1}^{n} \phi_i \log(\phi_i).$$

The graphs of GBC functions obtained by using our bivariate spline method will be presented. Thus, we have to divide the remaining of this section into a few subsections.

4.1 A New Biharmonic GBCs

Two different kinds of biharmonic GBCs were proposed and studied in [13] and [27], respectively. One is based on boundary element method (BEM) (cf. [27]) and one is based on finite element method (FEM). Both kinds of biharmonic GBCs fail to preserve the nonnegativity property. In this subsection, we shall use our minimization approach to define another kind of biharmonic GBC functions.

Let us use the following minimizing functional

$$f(\phi_1, \cdots, \phi_n) = \sum_{i=1}^{n} \frac{1}{2} \int_{p_n} |\Delta \phi_i|^2 dxdy \tag{38}$$

for (2) for our biharmonic GBCs. However, for computational efficiency, we instead use the following

$$\begin{aligned} \min_{\phi_i \in C^\infty(p_n)} \int_{p_n} |\Delta \phi_i|^2 dxdy \text{ subject to } & \phi_i(\mathbf{v}_j) = \delta_{ij}, j = 1, \cdots, n \\ & \phi_i(\mathbf{x}) \text{ is linear } \forall \mathbf{x} \in \partial p_n \\ & 0 \le \phi_i(\mathbf{x}) \le 1, \mathbf{x} \in p_n \end{aligned} \tag{39}$$

for each $i = 1, \cdots, n$. Similar to the proof of Theorem 1, we can show that there exists a unique minimizer ϕ_i. As this minimization is very similar to harmonic GBCs, the minimizers $s_i, i = 1, \cdots, n$ will satisfy (1) as discussed in the previous subsection. For completeness, we shall prove this fact later.

We now discuss how to compute the minimizer of (39) by using multivariate splines. That is, we consider

$$\begin{aligned} \min_{s_i \in S_d^r(\triangle)} \int_{p_n} |\Delta s_i|^2 dxdy \text{ subject to } & s_i(\mathbf{v}_j) = \delta_{ij}, j = 1, \cdots, n \\ & s_i \text{ is linear on all edges of } p_n \\ & 0 \le s_i \le 1 \text{ inside } p_n. \end{aligned} \tag{40}$$

To ensure the property: $0 \le s_i \le 1$ above, we shall use the alternating projection method discussed in the previous section. This is indeed possible because our spline functions are defined based on Bernstein-Bézier basis functions which possesses a partition of unit as discussed before. The projection of the spline functions which are nonnegative and less than or equal to 1 is simple to implement.

Let us now prove an existence and uniqueness result on the minimization (40).

Theorem 9 *Fix any spline space $S_d^r(\triangle)$ with $d \ge 3r + 2$ and $r \ge 2$. Then there exists a unique minimizer s_i of (40). Furthermore, all these s_i satisfy the GBC properties (1).*

Proof. First of all, since the solution from (**??**), say h_i satisfies the feasible set in (40), we know that the feasible set of (40) is not empty. Next the minimizing functional $F(s) = \int_\Omega |\Delta s|^2 dxdy$ is coercive. Indeed, let

$$\mathcal{S} = \{s \in S_d^r(\triangle) : 0 \le s \le 1, \int_{p_n} |\Delta s|^2 dxdy \le \int_{p_n} |\Delta h_i|^2 dxdy\}.$$

That is, the minimizer of (40) must be inside of the set $\mathcal{S}$ which is clearly a bounded set because each $s \in \mathcal{S}$ satisfies $0 \le s \le 1$.

Next we show the uniqueness of the minimizer. Otherwise, we will have to different spline functions u_1 and u_2 such that

$$m := \int_{p_n} |\Delta u_1|^2 dxdy = \int_{p_n} |\Delta u_2|^2 dxdy$$

where m is the minimum value of (39). It follows that $u_\alpha = \alpha u_1 + (1-\alpha)u_2$ is in the same spline space satisfying the feasible conditions in (40). Hence, we have $\int_{p_n} |\Delta u_\alpha|^2 dxdy \geq m$. In fact, we can show that $m = \int_{p_n} |\Delta u_\alpha|^2 dxdy$. Let $g(\alpha) = \int_{p_n} |\Delta u_\alpha|^2 dxdy$ be a constant. Then $g'(\alpha) = 0$ for all $\alpha \to 0_+$ implies that $\int_{p_n} \Delta u_1 \Delta u_2 dxdy = m$ and hence, $\Delta u_1 = \Delta u_2$. We see that $u_1 - u_2$ is a linear polynomial. The zero interpolation conditions on the boundary of p_n implies that $u_1 \equiv u_2$.

Let $s_i \in S_d^r(\triangle)$ be the minimizer for each i. We finally show that $(s_1, \cdots, s_n)$ will satisfy (1). Similar to the harmonic GBCs in the previous subsection, let $\Phi = s_1 + \cdots + s_n$. Then we can show that Φ is the unique minimizer of $\int_{p_n} |\Delta \Psi|^2 dxdy$ for $\Psi \in S_d^r(\triangle)$ satisfying boundary condition $\Psi = 1$ on ∂p_n. Clearly, 1 is also a minimizer and hence, $\Phi \equiv 1$. The other conditions in (1) can be shown in the same fashion. We have thus completed the proof. □

Next we discuss how to solve (40) numerically. In terms of spline space $S_d^r(\triangle)$ with $r \geq 2$, we know

$$\int_{p_n} |\Delta s_i|^2 dxdy = \mathbf{c}_i^\top B_\triangle \mathbf{c}_i,$$

if $s_i = \sum_{j=1}^N c_{ij} b_j$, where $\mathbf{c}_i = (c_{i1}, \cdots, c_{iN})^\top$ the spline coefficient vector of s_i and $B_\triangle$ is the bending matrix in the community of numerical PDEs whose entries are $\int_{p_n} \Delta b_j \Delta b_k dxdy$ for $j, k = 1, \cdots, N$. The constraints $0 \leq s_i \leq 1$ can be replaced by $0 \leq c_{ij} \leq 1$ for all $j = 1, \cdots, N$. The boundary conditions $s_i(\mathbf{x}) = g_i(\mathbf{x})$ for a continuous function g_i defined on the boundary ∂p_n can be enforced easily. We mainly use the projected gradient method discussed in the previous section to iteratively solving (40) numerically. Indeed, during our computation, we first use the harmonic GBCs as initial guesses as they satisfy the feasible conditions. We alternatively project the iterative solution to the feasible set and the discretized biharmonic equation until the errors are small, e.g. within $1e-3$. Our computational experiments show that when p_n is a convex domain, the minimizers of (40) can be approximated using any reasonably good triangulation and the linear constraints in (1) are satisfied very accurately, e.g. $1e-8$ over p_n and the minimizers are nonnegative. However, when p_n is not convex, the minimizers of (40) for each i are not easy to approximate and we have to use local refinement scheme at the re-entrance corner as shown in Figure 3. Once we use locally refined triangulations, the graphs of spline approximation of the minimizers are smooth and the spline minimizers are nonnegative and satisfy the linear constraints within a tolerance $1e-3$.

We now present an example of biharmonic GBCs.

Example 1 *Consider a polygon similar to the one in [1] as shown in Figure 3 (left). We use spline space $S_5^1(\triangle)$ with a triangulation shown in Figure 3 (left) to approximate biharmonic GBCs. Some of the graphs of these spline approximation of GBCs are shown in Figure* **??**. *We also check that they satisfy three constraints approximately with maximal errors* $(0.0053, 0.0028, 0.0033)$ *evaluated over 10,000 uniformly spaced points located within the polygon.*

These contour plots can be used to compared with all the GBCs discussed in [1]. Comparing with the contour lines of harmonic GBCs showed in [1], we can see that the biharmonic GBCs are more compactly supported than the corresponding harmonic GBC functions. We have to admit that the computational time for biharmonic GBC is more expensive than the time for harmonic GBCs. This is because when computing harmonic GBCs, we only need to solve linear systems while to compute

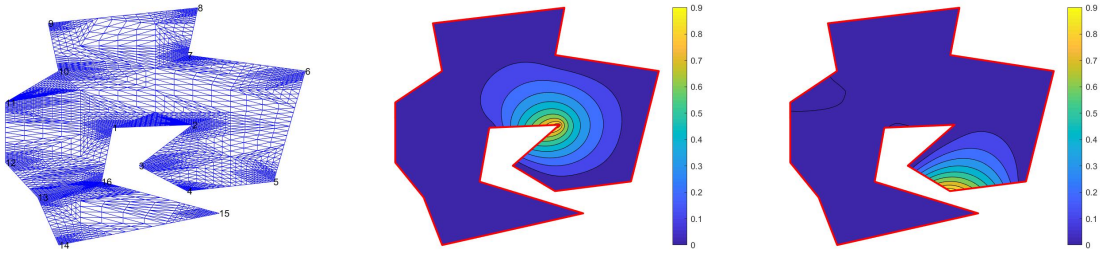

Figure 3: Triangulation of a domain similar to the domain in [1] and two biharmonic GBCs

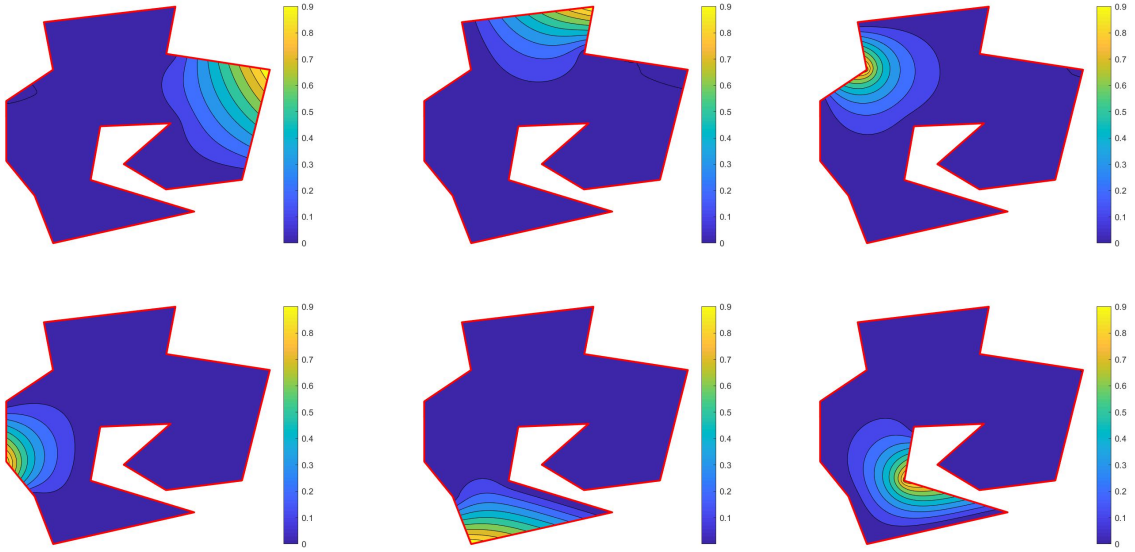

Figure 4: 6 biharmonic GBC functions over a domain similar to the one in [1]

biharmonic GBCs, we need to do iterative solutions. Also, the accuracy of constraints for harmonic GBCs is more accurate than that of biharmonic GBCs by using the same spline space.

Finally, let us discuss the limit of these $s_{i,\triangle} \in S_d^r(\triangle)$ as $|\triangle| \to 0$. Starting with an initial triangulation $\triangle$, let $\triangle_k$ be the kth uniform refinement of $\triangle$. It is known that $|\triangle_k| = |\triangle|/2^k$ and $S_d^r(\triangle_k) \subset S_d^r(\triangle_{k+1})$ for each $k \geq 0$. It follows that

$$\int_{p_n} |\Delta s_{i,\triangle_{k+1}}|^2 dxdy \leq \int_{p_n} |\Delta s_{i,\triangle_k}|^2 dxdy \tag{41}$$

for all $k \geq 0$. That is, $s_{i,\triangle_k}, k \geq 0$ are a bounded sequence in $H^2(p_n)$. By Rellich-Kondrashov theorem, there exists a subsequence from $s_{i,\triangle_k}, k \geq 0$ and its limit $s_i^* \in H^2(p_n)$. Without loss of generality, we may assume that the whole sequence converges, i.e.

$$s_{i,\triangle_k} \to s_i^*, \quad k \to \infty$$

weakly in $H^2(p_n)$ and strongly in $H^1(p_n)$. The boundedness of s_i^* in $H^2(p_n)$ implies that $s_i \in C(\overline{p_n})$, where $\overline{p_n}$ is the closure of p_n. We now show that s_i^* is the biharmonic GBC function ϕ_i which is the minimizer of (40). By Theorem 2, we know $S_d^r(\triangle_k), k \to \infty$ will be dense in $C^\infty(\overline{p_n})$. In fact, using the same ideas as the proof of Céa lemma, we can prove

$$\int_{p_n} |\Delta(s_{i,\triangle_k} - \phi_i)|^2 dxdy \leq \int_{p_n} |\Delta(Q_k(\phi_i) - \phi_i)|^2 dxdy \leq C|\triangle_k|^{2(d-1)} \to 0 \tag{42}$$

for a constant C dependent on ϕ_i as $k \to \infty$, where $d \geq 5$. Together with the boundary condition: $s_i^*|_{\partial p_n} = \phi_i|_{\partial p_n}$, we conclude that s_i^* is ϕ_i. Finally, let us explain some regularity of ϕ_i. According to the study on the interior regularity of Laplace equation(cf. [8]), we can show that $\phi_i \in H^{m+2}(q)$ for any open set $q \subset p_n$ for all $m \geq 0$. That is, we have

Theorem 10 *There exists a biharmonic GBC function ϕ_i satisfying $\phi_i|_{\partial p_n} = g_i$ and $0 \leq \phi_i \leq 1$. Furthermore, ϕ_i is $H^m_{loc}(p_n)$ for any integer $m \geq 1$. Finally, all these $\phi_i, i = 1, \cdots, n$ satisfy the GBC conditions (1).*

Proof. Let us outline a proof here while leaving the detail to the interested reader. For any open set $q \subset p_n$ strictly contained in p_n, i.e., $q \subset p_n$, but $q \neq p_n$, let $\widetilde{q} \subset p_n$ be another open set strictly contained in p_n, but contain q. That is, $q \subset \widetilde{q} \subset p_n$. Define a cutoff function $\zeta \in C^\infty(\mathbb{R}^2)$ such that $\zeta(\mathbf{x}) = 1$ when $\mathbf{x} \in q$, $\zeta(\mathbf{x}) = 0$ when $\mathbf{x} \in \mathbb{R}^2 \backslash \widetilde{q}$, and between 0 and 1 when $\mathbf{x} \in \widetilde{q} \backslash q$. Next we define central difference operators

$$D^2_{x,h} f(x,y) = \frac{f(x+h,y) - 2f(x,y) + f(x-h,y)}{2h^2}$$

for $h > 0$ and similar for $D^2_{y,h} f(x,y)$. When $h > 0$ is sufficiently small, we have

$$v = D^2_{x,h}(\eta^2 (D^2_{x,h} s_i)) \in H^2(p_n) \text{ and } v|_{\partial p_n} = 0.$$

It follows that

$$\begin{aligned} 0 &= \int_{p_n} \Delta s_i \Delta v dxdy \\ &= \int_{p_n} D^2_{x,h}(\Delta s_i) \Delta[\zeta^2 D^2_{x,h} s_i] dxdy \\ &= \int_{p_n} D^2_{x,h} \Delta s_i \Delta[\zeta^2] D^2_{x,h} s_i dxdy + \int_{p_n} D^2_{x,h} \Delta s_i \zeta^2 D^2_{x,h} \Delta s_i dxdy. \end{aligned} \tag{43}$$

By Cauchy-Schwarz inequality, we use the above equality to have

$$\begin{aligned}\int_{p_n} D^2_{x,h}\Delta s_i\zeta^2 D^2_{x,h}\Delta s_i dxdy =& -\int_{p_n} D^2_{x,h}\Delta s_i\Delta[\zeta^2]D^2_{x,h}s_i dxdy\\ \leq& 2\left(\int_{p_n} D^2_{x,h}\Delta s_i\zeta^2 D^2_{x,h}\Delta s_i dxdy\right)^{1/2}\left(\int_{p_n}|\Delta\zeta|^2|D^2_{x,h}s_i|^2 dxdy\right)^{1/2}.\end{aligned}$$

Similifying the above inequality leads to

$$\int_{p_n} D^2_{x,h}\Delta s_i\zeta^2 D^2_{x,h}\Delta s_i dxdy \leq 4\int_{p_n}|\Delta\zeta|^2|D^2_{x,h}s_i|^2 dxdy.$$

Since $\zeta^2 = 1$ on q and let $C = 4\|\Delta\eta\|_{\infty,p_n}$ which is dependent on q, we have

$$\int_q |D^2_{x,h}\Delta\phi_i|^2 dxdy \leq \int_{p_n} D^2_{x,h}\Delta\phi_i\zeta^2 D^2_{x,h}\Delta\phi_i dxdy \leq C\int_{p_n}|D^2_{x,h}\phi_i|^2 dxdy \tag{44}$$

for all $h > 0$ sufficiently small. Similar for $\int_q |D^2_{y,h}\Delta\phi_i|^2 dxdy \leq C\int_{p_n}|D^2_{y,h}\phi_i|^2 dxdy$. Letting $h \to 0_+$, we have

$$\int_q |\Delta^2\phi_i|^2 dxdy \leq C\int_{p_n}|\Delta\phi_i|^2 dxdy < \infty.$$

Hence, $\phi_i \in H^4_{loc}(p_n)$ because the boundedness on the left-hand side of the above inequalities and the boundedness $\|\phi_i\|_{L^2(p_n)}$ imply the boundedness of all derivatives of order between 1 and 4. The above arguments can be repeated for higher order. This finishes the proof of $\phi_i \in H^{m+2}_{loc}(p_n)$ for $m \geq 0$. □

4.2 Square GBCs

For $f(\phi_1,\cdots,\phi_n) = \sum_{i=1}^n \int_{p_n}|\phi_i(\mathbf{x})|^2 d\mathbf{x}$, we replace it by $F(\mathbf{c}_1,\cdots,\mathbf{c}_n) = \sum_{i=1}^n \|\mathbf{c}_i\|^2$ as we know

$$A_1\|\mathbf{c}_i\|_\infty \leq \|s_i\|_{\infty,p_n} \leq A_2\|\mathbf{c}_i\|_\infty \tag{45}$$

for two positive constants A_1, A_2 which is dependent on the quasi-uniformality γ of the underlyging triangulation $\triangle$, according to the study in [18]. Thus, we recast the minimization in (9) with F given by

$$F(\mathbf{c}_1,\cdots,\mathbf{c}_n) = \sum_{i=1}^n \|\mathbf{c}_i\|^2. \tag{46}$$

Then we use spline space $S^2_8(\triangle)$ with $|\triangle| = 0.1$ and apply Algorithm 4 to find these GBC functions. The side constraints (1) are satisfied within error $1e-3$. See graphs as shown in Figure 5. We have also use a spline space $S^3_{11}(\triangle)$ and $S^4_{16}(\triangle)$. Their graphs are similar to those in Figure 5.

4.3 Maximum Entropy GBC Functions

The maximum entropy GBC was invented in [24] and studied in [15], and [9]. The authors used the minimization to establish the existence of the GBC. However, the solution is not explicitly given. One has to solve two nonlinear equations which may be done by using Newton's method. According to our recipe in the previous section, we can reformulate it as follows:

$$\min_{\phi_1,\cdots,\phi_n\in C^\infty(p_n)} \sum_{i=1}^n \phi_i\log(\phi_i+\epsilon) : \text{subject to (1)}, \tag{47}$$

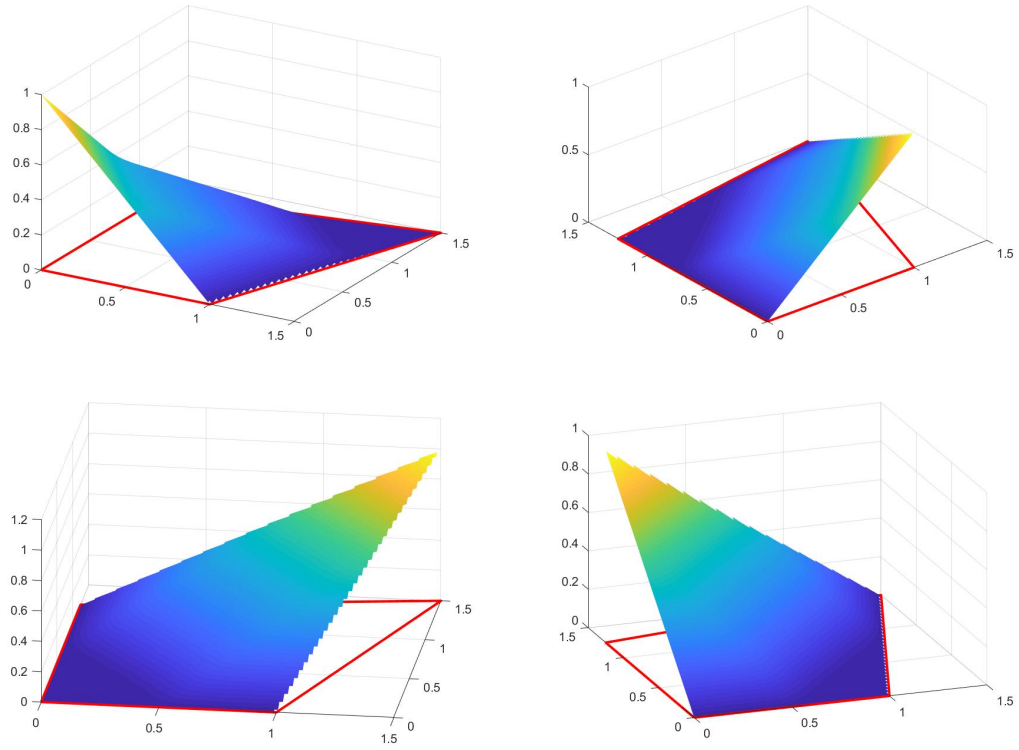

Figure 5: Four GBC functions over a quadrilateral based on the minimizing functional F in (46)

where $\epsilon \geq 0$. Note that when $\epsilon = 0$, the solution is the maximum entropy GBC discussed in [24] and [15]. Clearly, $f(\phi_1, \cdots, \phi_n, \epsilon) = \sum_{i=1}^{n} \phi_i \log(\phi_i + \epsilon)$ is a strictly convex function. By using Theorem 1, there exists a unique set of minimizers $\phi_1, \cdots, \phi_n$ for each $\epsilon > 0$. For simplicity, we shall call them ϵ-maximum entropy GBC. When $\epsilon = 0$, the minimizers are exactly one in [24]. We now discuss how to find those functions numerically.

By using (45), we use

$$F(\mathbf{c}_1, \cdots, \mathbf{c}_n) = \sum_{i=1}^{n} \sum_{j=1}^{N} c_{ij} \log(c_{ij} + \epsilon) \tag{48}$$

to be the minimizing functional for (15). Our implementation is exactly the same as the one in the previous subsection except for using the $F(\mathbf{c}_1, \cdots, \mathbf{c}_n)$ in this subsection instead of $F(\mathbf{c}_1, \cdots, \mathbf{c}_n) = \sum_{i=1}^{n} \|\mathbf{c}_i\|^2$. Again we use spline space $S_8^2(\triangle)$ with a good triangulation with $|\triangle|$ small enough. The graphs of these ϵ-minimal entropy GBC are given in Figure 6 over a pentagon p_5. The graphs are almost the same as the one in the previous subsection, where $\epsilon = 0.01$.

5 Some Applications of GBC functions

In this section, we present a few examples to show an interpolatory surface, polygonal deformation, and image enhancement using the GBCs obtained by the computational method proposed in this paper. For convenience, we simply use harmonic GBCs which can be done much faster than other GBCs. Consider the following polygon with 20 sides shown in Figure 7 together with a triangulation. We use continuous splines of degree 8 based on the triangulation to approximate the harmonic GBCs.

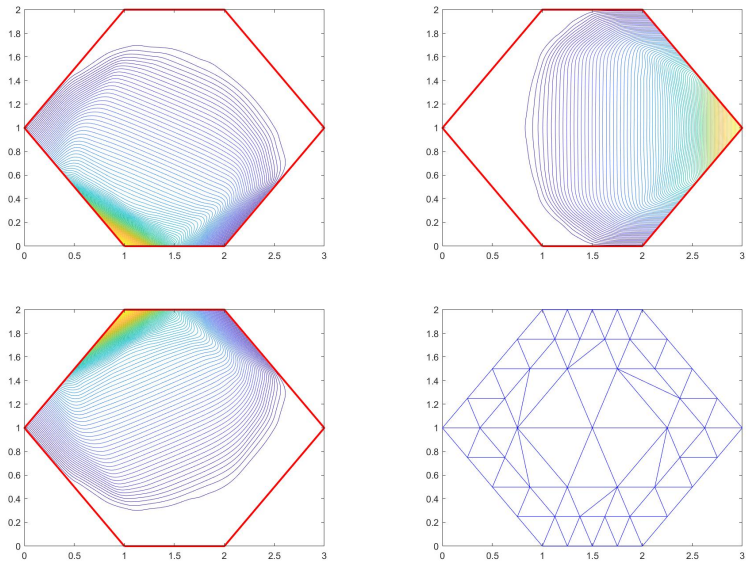

Figure 6: Three ϵ-minimal entropy GBC functions over a hexagon with a triangulation shown based on the minimizing functional F in (48). The other three are a rotated version of these three shown.

The resulting surfaces are plotted in contour lines which are clearly very smooth. The contour lines are at values $1e-6, 1e-5, 1e-4, 1e-3, 1e-2, 0.02, 0.04, ..., 1$. Let us present the contour lines of each GBC functions in Figures 8–12. Once we obtain these 20 GBC functions, we interpolate a simple function x^2+y^2 at the vertices of the polygon to obtain the graph on the right of Figure 7.

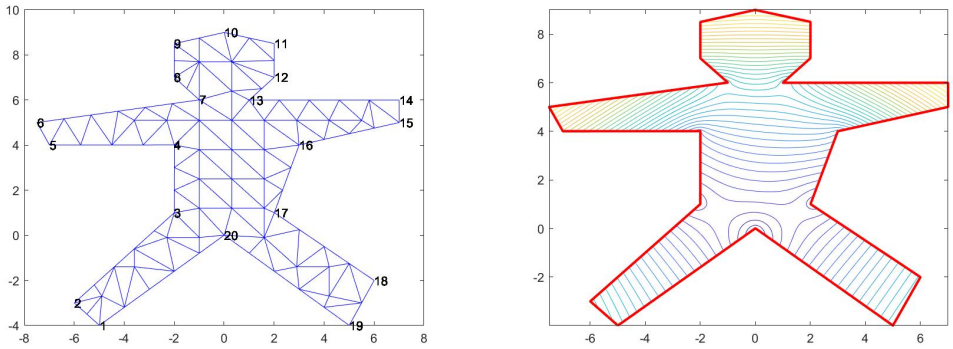

Figure 7: A polygon with a triangulation and the contour lines of an interpolatory surface

Next we present a polygon deformation. Let us begin with the polygon shown in Figure 7. We deform it to another polygon as shown in Figure 13. That is, for each $\mathbf{x} \in p_n$ with vertices $\mathbf{v}_1, \cdots, \mathbf{v}_n$, we have GBCs $\phi_i(\mathbf{x}), i = 1, \cdots, n$. For a new polygon $\tilde{p}_n$ with vertices $\mathbf{u}_1, \cdots, \mathbf{u}_n$, we simply plot new point $\sum_{i=1}^{n} \phi_i(\mathbf{x})\mathbf{u}_i$ together with the value $f(\mathbf{x})$.

Finally, we present an application of image enhancement. Let us consider a picture of of the logo of Hangzhou Dianzi University in Figure 14. The center piece is the sculpture of Tripod. We chose a pentagon P_5 to include the tripod on the left to generate 5 GBC functions and then extend the image values within P_5 to a larger pentagon $\widetilde{P}_5$ shaded as shown on the right of Figure 14 by using bivariate

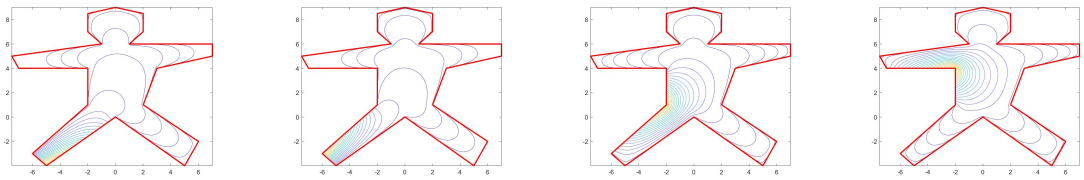

Figure 8: Four harmonic GBC functions over the polygon p_{20} shown in Figure 7.

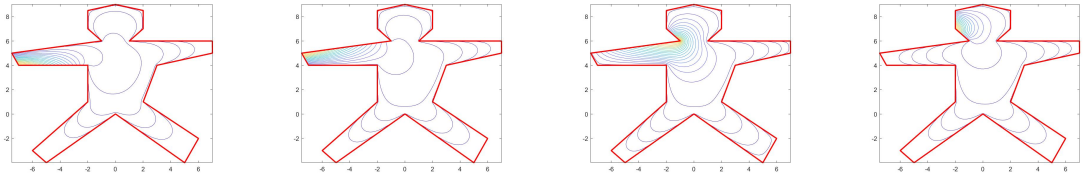

Figure 9: Four harmonic GBC functions over the polygon p_{20} shown in Figure 7.

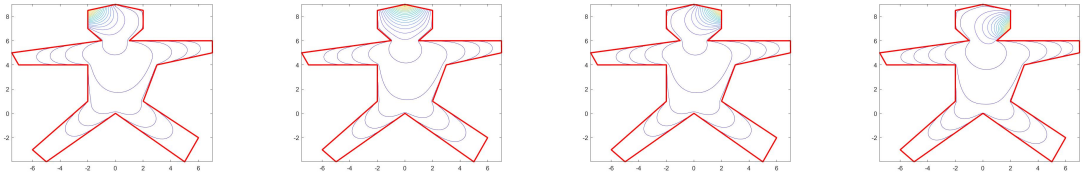

Figure 10: Four harmonic GBC functions over the polygon p_{20} shown in Figure 7.

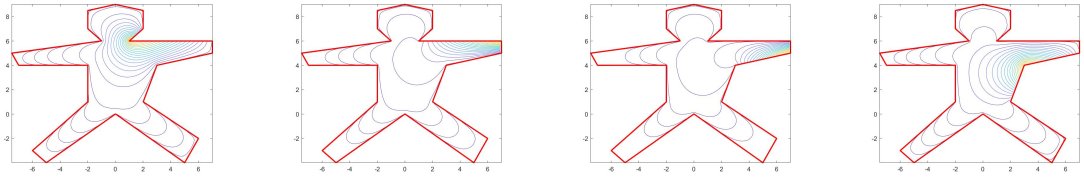

Figure 11: Another four harmonic GBC functions over the polygon p_{20} shown in Figure 7.

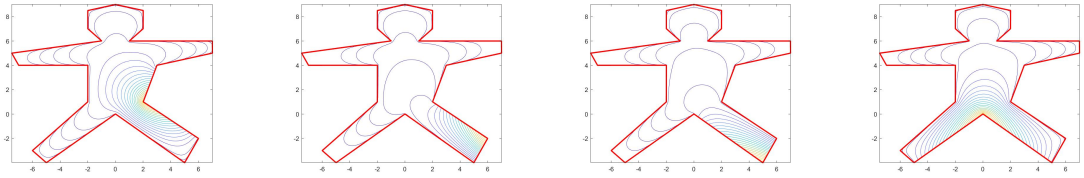

Figure 12: Last four harmonic GBC functions over the polygon p_{20} shown in Figure 7.

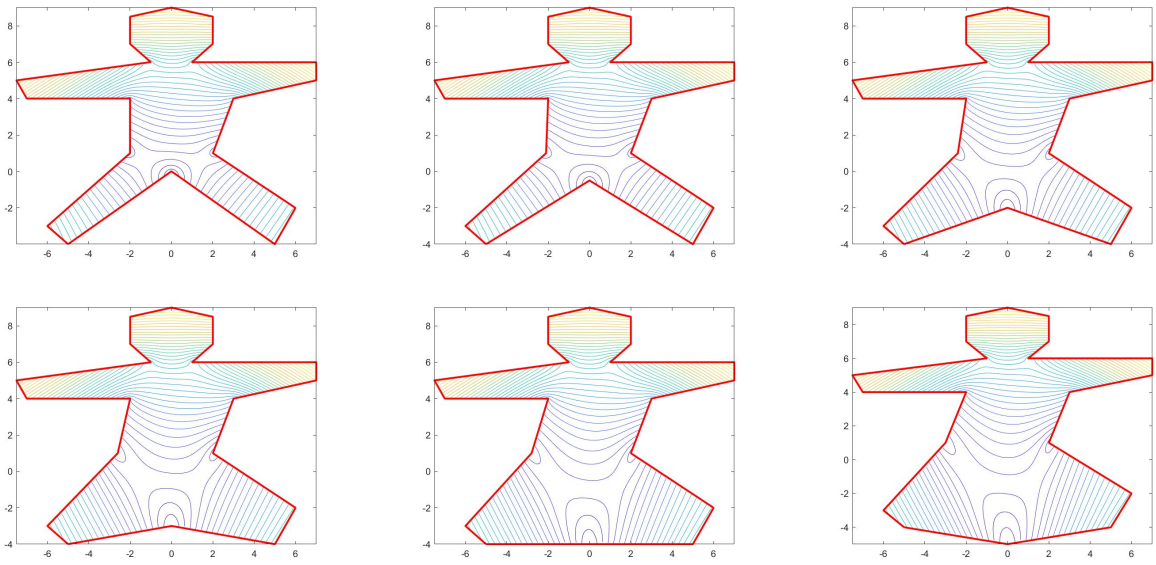

Figure 13: The polygon p_{20} shown on the most left of the first row is deformed to the polygon (the last one) in the second row.

spline function data fitting method. The spline data fitting method is to fit the given image values at the new locations which are linear combinations of the GBC values with new vertices $\widetilde{P}_5$ and then evaluate the fitting splines at all the pixel locations within the new pentagon to have a new image shown on the right-hand side of Figure 14.

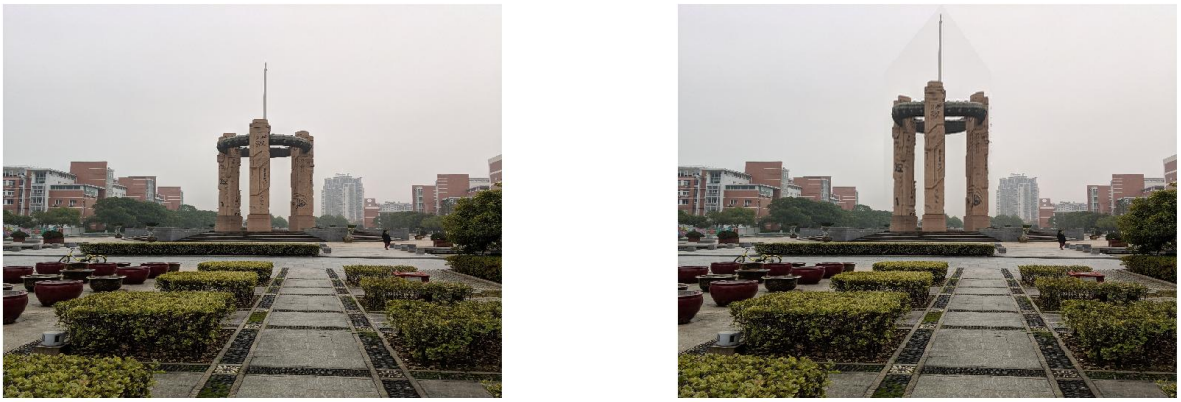

Figure 14: An Image of Hangzhou Dianzi University with the Sculpture of Tripod (left) and an Enhanced Image with shaded pentagon (right)

6 Conclusion and Remarks

We have established a minimization approach to define new GBC functions which is more general than the harmonic, biharmonic, and minimal entropy GBCs. We successfully implemented bivariate

smooth spline functions to approximate the minimizers and obtain good approximations of the new and existing GBCs. They are very convenient for various GBC applications as presented in the previous section. We plan to extend the computation, mainly the computation based on bivariate smooth splines to the 3D setting using trivariate smooth spline functions developed in [3]. More results will be reported in near future. In addition, we plan to use the minimization (2) based on $f(\phi_1, \cdots, \phi_n) = \sum_{i=1}^n \int_{p_n} |\phi_i(\mathbf{x})| d\mathbf{x}$ to construct more interesting GBC functions. Finally, during our study, we found that when p_n is convex, the minimization (39) produces nonnegative GBC functions without using the non-negativity constraint. We plan to study this conjecture.

References

[1] D. Anisimov, Barycentric coordinates and their properties, in *Generalized Barycentric coordinates in Computer Graphics and Computational Mechanics*, edited by K. Hormann and N. Sukuma, CRC Press, 2018.

[2] H. Attouch and J. Peypouquet, The rate of convergence of Nesterov's accelerated forward-backward method is actually faster than $1/k^2$, SIAM J. Optim. 26(2016), 1824–1834.

[3] G. Awanou, M. -J. Lai, and P. Wenston. The multivariate spline method for scattered data fitting and numerical solution of partial differential equations. In Wavelets and splines: Athens 2005, pages 24–74. Nashboro Press, Brentwood, TN, 2006.

[4] A. Beck and M. Teboulle, A Fast Iterative Shrinkage-Thresholding Algorithm for Linear Inverse Problems, SIAM J. Imaging Sciences, Vol. 2 (2009), pp. 183–202.

[5] W. Deng, M. -J. Lai, Z. Peng, and W. Yin, Parallel Multi-Block ADMM with $o(1/k)$ Convergence, J. Scientific Computing, vol. 71 (2017) pp. 712–736.

[6] F. Deutsch, Best Approximation in Inner Product Spaces, Canadian Mathematical Society, 2001.

[7] F. Deutsch, a private communication, Dec. 18, 2018.

[8] L. C. Evans, Partial Differential Equations, American Math. Soc., 1998.

[9] M. Floater, Generalized barycentric coordinates and applications, Acta Numerica, 24 (2015), 161–214.

[10] M. Floater and M. -J. Lai, Polygonal spline spaces and the numerical solution of the Poisson equation, SIAM Journal on Numerical Analysis, (2016) pp. 797–824.

[11] Von Golitschek, M., Lai, M. -J. and Schumaker, L. L., Bounds for Minimal Energy Bivariate Polynomial Splines, Numerische Mathematik, vol. 93 (2002) pp. 315–331.

[12] K. Hormann and N. Sukumar, Generalized Barycentric Coordinates in Computer Graphs and Computational Mechanics, CRC Press, 2018.

[13] A. Jacobson, I. Baran, J. Popovic, and O. Sorkine, Bounded biharmonic weights for real-time deformation, ACM Trans. Graph. 30 (4): 78 (2011).

[14] P. Joshi, M. Meyer, T. DeRose, B. Green, and T. Sanocki, Harmonic Coordinates for Character Articulation, Pixar Technical Memo#06–02b, Pixar Animation Studio, 2006.

[15] K. Hormann and N. Sukumar, Maximum entropy coordinates for arbitrary polytopes, in Symposium on Geometry Processing 2008, Eurographics Association, pp. 1513–1520.

[16] M. -J., Lai, and Lanterman, J., A polygonal spline method for general 2nd order elliptic equations and its applications, in Approximation Theory XV: San Antonio, 2016, Springer Verlag, (2017) edited by G. Fasshauer and L. L. Schumaker, pp. 119–154.

[17] M. -J. Lai and Schumaker, L. L., Approximation Power of Bivariate Splines, Advances in Computational Mathematics, vol. 9 (1998) pp. 251–279.

[18] M. -J. Lai and L. L. Schumaker, *Spline Functions over Triangulations*, Cambridge University Press, 2007.

[19] James Lanterman, Construction of Smooth Vertex Splines over Quadrilaterials, Ph.D. Dissertation, the University of Georgia, Summer, 2018.

[20] G. Manzini, A. Russo, N. Sukumar. New perspectives on polygonal and polyhedral finite element methods. Math. Models Methods Appl. Sci., 24(8): 1665–1699, 2014.

[21] Y. E. Nesterov, A method for solving the convex programming problem with convergence rate $O(1/k^2)$, Dokl. Akad. Nauk SSSR, 269 (1983), pp. 543–547 (in Russian).

[22] Y. Nesterov, Introductory Lectures on Convex Optimization, Kluwer Academic Publications, Mass. USA, 2004.

[23] A. Rand, A. Gillette, C. Bajaj. Quadratic serendipity finite elements on polygons using generalized barycentric coordinates. Math. of computation, 83(290): 2691–2716, 2014.

[24] N. Sukumar (2004), Construction of polygonal interpolants: a maximum entropy approach, Int. J. Numer. Meth. Engng 61, 2159–2181.

[25] N. Sukumar and A. Tabarraei (2004), Conforming polygonal finite elements, Int. J. Numer. Meth. Engng 61, 2045–2066.

[26] E. L. Wachspress, A Rational Finite Element Basis, Math. Sci. Eng. 114, Academic, New York, 1975.

[27] O. Web, R. Poranne, and G. Gotsman, Computer Graphics Forum, 31(2012), pp. 2409–2422.

[28] J. Zhang, B. Deng, Z. Liu, G. Patané, S. Bouaziz, J. Hormann, and L. Liu, Local Barycentric Coordinates, SIGGRAPH, Asia, 2014.